

# Flexible Energy Conversion Control Strategy for Brushless Dual-Mechanical-Port Dual-Electrical-Port Machine in Hybrid Vehicles

Xun Han, *Student Member, IEEE*, Wubin Kong, *Member, IEEE*, Ronghai Qu, *Fellow, IEEE*, Dawei Li, *Member, IEEE*, Tianjie Zou, *Student Member, IEEE*, Xiang Ren, *Student Member, IEEE*, Tonghao Pei, *Student Member, IEEE*, Kai Yang, and Chun Gan, *Member, IEEE*

**Abstract**—Due to the advantages of high torque density and compact mechanical structure, brushless dual-mechanical-port dual-electrical-port (BLDD) PM machine has become a promising alternative in series-parallel HEVs. However, two sets of windings in the same core may also result in flux cross coupling, which deteriorate control performance. Through special design of the magnetic circuit, the two sets of windings in the stator side are decoupled. In this paper, the mathematical model of BLDD-PM machine is analyzed firstly. Then, based on energy management system and the model of machine, the decoupled vector control algorithm for outer and inner rotor is developed. Next, common operation states under city road condition for hybrid vehicles have been summarized. According to operation state of HEV, the power flow analysis in the BLDD-PM machine system has been done. To validate the analysis results, experimental test under different operation condition has been conducted. Test results show good control performance of the BLDD-PM prototype and verify the correctness of analysis.

**Index Terms**—BLDD-PM machine, power flow analysis, HEV.

## I. INTRODUCTION

Today, in the background of energy saving and high efficiency, hybrid electrical vehicles (HEV) has aroused wide concern from both academic circle and industry due to its high energy efficiency, energy diversity and clean characteristics [1]–[2]. Since there are two source of energy supply (i.e. fuel energy and electrical energy) in the car, energy distribution device has played a dominant role under the whole HEV operation process. Conventionally, in traditional automotive drive system, automatic transmission usually with the continuous variable transmission (CVT) has acted as a power transmission system. However, in HEV drive system, internal-combustion engine (ICE), electrical motor and generator constitute a new type of transmission device, which is also called electrical CVT (e-CVT) [3]–[4]. The power-splitting device of e-CVT is normally designed to a planetary gearbox, allocating the power flow of ICE and

battery to drive the whole system efficiently. The whole scheme of typical single-mode transmission is shown in the Fig. 1. It is worth mentioning that this structure has been first used in Toyota Prius hybrid models and achieved great commercial success.

To replace planetary gearbox, and further improve the system operation efficiency, the concept of four-quadrant transducer (4QT) concept was proposed in [5]–[7] to operate the ICE independent of road load condition. The 4QT system concept diagram is illustrated in Fig. 2. Though these conventional dual rotor machines possess the advantages such as high compactness and high power density, but undeniably, windings should be placed on the rotor, which means brushes and slip rings must be used in dual mechanical port (DMP) machines [8]–[10]. These brushes and slip rings will inevitably reduce the system reliability thus increasing maintenance cost.

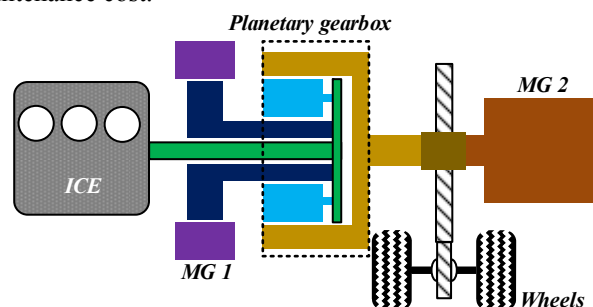


Fig. 1. Conventional hybrid power system.

To get rid of the negative influence brought by brushes and slip rings, a new DMP machine type named brushless dual-mechanical-port dual-electrical-port (BLDD) PM machine was proposed and analyzed based on previous concept and work [11]. This type of machine is usually designed on the basis of the flux modulation theory [12]–[17]. The whole machine can be regarded as a magnetic geared machine (MGM) and a regular PMSM machine cascaded through mechanical shaft [18]. The brushes and slip rings are eliminated and the rotor armature winding is moved to stator. In [19]–[20], the MGM and PMSM parts are separated in axial direction, and the control of this system is investigated in [21]–[26]. In addition, the two parts can be integrated into one frame [27]–[29], and this structure is more compact. Recently, a new BLDD machine topology with spoke array magnets in flux modulator is proposed to further improve torque density of this machine [30]. Due to the special magnetic circuit

Manuscript received Feb. 7th, 2018; revised Apr. 27th, 2018; accepted Jun. 29, 2018. This work was supported by the National Key Research and Development Program of China under project 2017YFB0102300, the National Natural Science Foundation of China under Project 51607078, the Fundamental Research Funds for the Central Universities under project 2018KFYYXJJ070, and grants from the Power Electronics Science and Education Development Program of Delta Environmental & Educational Foundation DREM2016001. (Corresponding author: Wubin Kong.)

The authors are with the State Key Laboratory of Advanced Electromagnetic Engineering and Technology, School of Electrical and Electronic Engineering, Huazhong University of Science and Technology, Wuhan 430074, China (e-mail: [hex@hust.edu.cn](mailto:hex@hust.edu.cn); [wubinkong@126.com](mailto:wubinkong@126.com)).

design, the torque capability of the PMSM part in the proposed machine is increased significantly.

Although there are many papers discuss the topology of the BLDD machine, energy distribution state or control strategy of this new type e-CVT under HEVs different operation conditions has not been well studied. The analysis of two kinds of energy flow and control strategy are the basis for this machine to get practical application in the HEVs, and they are also the core focus of BLDD-PM machine drive system.

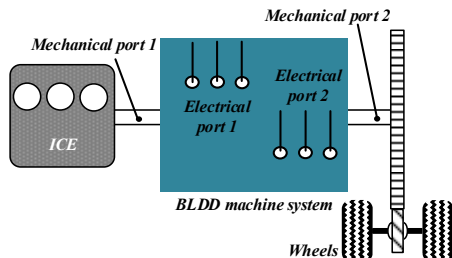


Fig. 2. The four-quadrant transducer concept diagram.

In this paper, the operation characteristics of a newly type topology machine is investigated. Based on the BLDD-PM machine operation principle and external characteristic analysis, a basic control algorithm is developed for this machine. The machine structure and operation principle will be introduced in Section II. Section III will focus on energy flow under different operation condition. Then, Section IV will be devoted to design basic vector control algorithm. Finally, based on the newly type experiment prototype of BLDD-PM machine, experimental validation of will be given in Section V.

## II. MACHINE STRUCTURE AND OPERATION PRINCIPLE

As mentioned before, BLDD machine plays the role of the core component during the whole energy conversion process in the HEV. Generally, there are three types of HEV, i.e., series structure, paralleled structure and series-parallel structure. From the operation principle, the proposed BLDD machine system can be divided into series-parallel structure. The typical structure of series-parallel HEV has been shown in Fig. 1. However, different from the conventional series-parallel structure, the inner rotor of the BLDD machine is coupled with output rotor through an electromagnetic gear rather than mechanical one. So the modulation winding should be excited with proper current to maintain the function of electromagnetic gear when the ICE works. To get a better understanding of this machine, its structure and working principles are introduced firstly.

### A. Machine structure

As mentioned before, a BLDD-PM machine is composed of one MGM and one regular PMSM. The structure of experiment used machine in this paper is shown in Fig 3. It is noteworthy that two machine parts, i.e. MGM part and PMSM part, have already been placed into one machine frame. The purpose of split tooth stator adopted in this machine is to separate two sets of windings and reduce coupling effect between them. The spoke array structure in modulation ring is

proposed to focus flux thus reducing magnetic flux leakage and further increasing the torque density of the system.

Besides, in this topology, permanent magnets have been placed both in the two rotors, so the modulator rotor and PM rotor name which are often used in conventional BLDD-PM

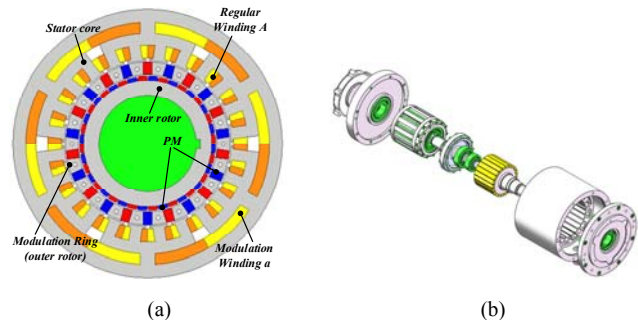


Fig. 3. BLDD-PM machine diagram. (a). Machine cross-section. (b). Prototype for proposed BLDD-PM machine.

machine are called outer rotor and inner rotor instead. In the stator side, there are two sets of windings referred to as modulation winding and regular winding, respectively. To decouple the two sets of windings, the windings displacement is presented as the Fig. 4, which takes phase A for example. From the final effect, the coupling between the two sets of windings can be regarded as the equivalent circuit Fig. 5. Specifically, the modulation winding is composed of the two section windings A and A', and they are connected in series. The flux linkage of mutual inductance direction is marked in the picture, the flux produced by the regular winding links with the A and A' in different direction. So the total effect of coupling is impaired significantly. The detailed design parameters listed in Table I.

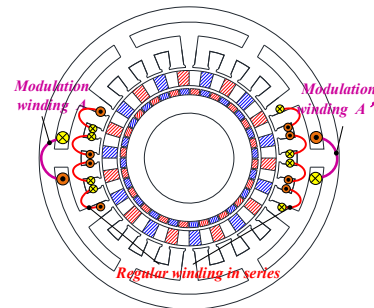


Fig. 4. Winding connection for phase A.

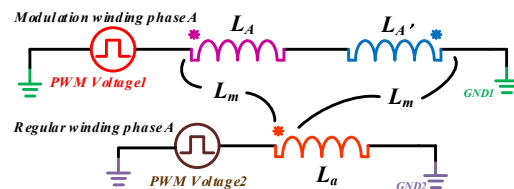


Fig. 5. Equivalent circuit of the two sets of winding.

TABLE I  
 MAIN PARAMETERS OF THE PROTOTYPE

Item	Value
Outer rotor rated speed, rpm	1000
Inner rotor rated speed, rpm	1000
Outer rotor rated torque, Nm	8
Inner rotor rated torque, Nm	13.5
Outer rotor rated phase current, A	48.5
Inner rotor rated phase current, A	8.5
Modulation winding rated phase voltage, V	35
Regular winding rated phase voltage, V	50
Stator outer diameter, mm	210
Stator inner diameter, mm	130
Stack length, mm	100
Air-gap length, mm	1
Number of modulation winding pole pairs	2
Number of regular winding pole pairs	11
Outer rotor pole pairs	22
Inner rotor pole pairs	20

### B. Operation principles

Since there are two electrical ports and two mechanical ports in the BLDD machine, the torque and speed relation of the rotors and stators is far more complicated than normal one electrical port and one mechanical port machine. For the convenience of analysis in this paper, the positive directions of speed and electromagnetic torque are set along a counterclockwise direction.

Due to the “magnetic gearing effect” [14]~[17], the pole number of the stator, outer rotor and inner rotor should satisfy such relationship (1) to produce stable electromagnetic torque.

$$p_{wm} = p_{ro} - p_{ri} \quad (1)$$

where  $p_{wm}$ ,  $p_{ro}$  and  $p_{ri}$  are the pole pair number of modulation winding, outer rotor and inner rotor, respectively. For the machine shown in Fig. 3, slots  $Z=12$ ,  $p_{ri}=20$ ,  $p_{wm}=2$  and the pole ratio  $k$  is defined as the ratio of  $p_{ri}$  to  $p_{wm}$ , that is 10. In the flux modulation machine, here it should be noted that the concept of pole ratio is similar to gear ratio in the gear system.

From the final effect, it can be concluded that the torque of the outer rotor is formed by two parts: one can be called MGM part which represents the force produced by magnetic gear machine; the other is PMSM part, which means the force produced by conventional PMSM motor.

For MGM part, firstly, magnetic field is produced by the current of modulation winding with  $p_{wm}$  pole pair number. Then, this magnetic field with  $p_{wm}$  pole pair number is converted to pole pair number of  $p_{ri}$  after modulated by the rotating outer rotor. Finally, this magnetic field with pole pair number of  $p_{ri}$  can couple with inner rotor to produce steady torque. To be more specifically, the electrical frequency of the three parts is always balanced by equation (2). And the equation can be further expressed in mechanical angular speed form as (3). Substitute (1) into (3), the final expression is written in (4).

$$f_{wm} = f_{ro} - f_{ri} \quad (2)$$

$$\Omega_{wm} \cdot p_{wm} = \Omega_{ro} p_{ro} - \Omega_{ri} p_{ri} \quad (3)$$

$$\frac{\Omega_{ro} - \Omega_{wm}}{\Omega_{ri} - \Omega_{ro}} = \frac{p_{ri}}{p_{wm}} = k \quad (4)$$

where  $f_{wm}$ ,  $f_{ro}$  and  $f_{ri}$  are the electrical frequency of modulation winding, outer rotor and inner rotor, respectively.  $\Omega_{wm}$ ,  $\Omega_{ro}$  and  $\Omega_{ri}$  are corresponding mechanical angular speed. In fact, if modulator rotor (outer rotor) is fixed, i.e.  $f_{ro}=0$ , the MGM can be regarded as a PM Vernier machine. Moreover, the MGM can be regarded as a conservative system, and the torque balance equation and the energy conservation equation can be written as (5) (6) (7).

$$T_{wm} + T_{rom} + T_{rim} = 0 \quad (5)$$

$$T_{wm} \cdot \Omega_{wm} + T_{rom} \cdot \Omega_{ro} + T_{rim} \cdot \Omega_{ri} = 0 \quad (6)$$

$$T_{ri} = T_{rim} \quad (7)$$

where  $T_{rom}$  is MGM torque components on the outer rotor;  $T_{ri}$  and  $T_{rim}$  are the total torque input by ICE shaft and MGM torque components of the inner rotor, respectively. Then, the torque relation of the three parts can be deduced from (1) (3) (5) (6), the final result is shown in (8) and (9). It is not difficult to find out from equation (4), (8) and (9) that the MGM can be totally equivalent to a planetary gear planetary gear mechanism. The only difference is that MGM motion parts are connected through magnetic field instead of mechanical connection.

$$T_{rom} = -\frac{k+1}{k} T_{rim} = -\frac{p_{ro}}{p_{ri}} T_{rim} \quad (8)$$

$$T_{wm} = \frac{1}{k} T_{rim} = \frac{p_{wm}}{p_{ri}} T_{rim} \quad (9)$$

As for PMSM part, the electrical frequency relationship of the conventional winding and outer rotor are the same as a regular PMSM machine since the conventional winding and the outer rotor can be regarded as an equivalent regular PMSM. The frequency relationship is shown in (10) and the total torque of the outer rotor can be expressed as (11).

$$f_{wr} = f_{ro} = \frac{n_{ro} \cdot p_{ro}}{60} \quad (10)$$

$$T_{ro} = T_{rom} + T_{ror} \quad (11)$$

where  $f_{wr}$  and  $n_{ro}$  are the electrical frequency of regular winding, speed of the outer rotor, respectively;  $T_{ro}$  and  $T_{ror}$  are total and PMSM torque components of the outer rotor, respectively. The design purpose of regular winding electric port is to increase the total torque of the outer rotor and return extra energy to DC bus.

The power relationship of the two rotors and windings can be summarized as (12)~(16). Here  $P_{ri}$ ,  $P_{e\_wm}$ ,  $P_{e\_wr}$  and  $P_{ro}$  represent the power of inner rotor, modulation winding, regular winding and outer rotor respectively.

$$P_{ri} = T_{ri} \cdot \Omega_{ri} \quad (12)$$

$$P_{ro} = T_{ro} \cdot \Omega_{ro} \quad (13)$$

$$P_{e\_wr} = T_{ror} \cdot \Omega_{ro} \quad (14)$$

$$P_{e\_wm} = T_{wm} \cdot \Omega_{wm} \quad (15)$$

$$P_{ri} = P_{ro} + P_{e\_wm} + P_{e\_wr} \quad (16)$$

### III. DESIGN OF CONTROL ALGORITHM

#### A. PMSM high frequency vibration analysis

As mentioned before, through special magnetic circuit design, the two windings are decoupled and cross coupling component is deduced to a relatively low level. For the convenience of deduction, the coupling effect can be neglected. Based on this premise, the flux linkage equations in  $d$ - $q$  reference frame can be written as (17), where the subscript  $-wm$  represents variables of the modulation winding and  $-wr$  represents variables of the regular winding.

$$\begin{pmatrix} \Psi_{d\_wm} \\ \Psi_{q\_wm} \\ \Psi_{d\_wr} \\ \Psi_{q\_wr} \end{pmatrix} = \begin{pmatrix} L_{d\_wm} & M_{dq\_wm} \\ M_{dq\_wm} & L_{q\_wm} \\ & & L_{d\_wr} & M_{dq\_wr} \\ & & M_{dq\_wr} & L_{q\_wr} \end{pmatrix} \begin{pmatrix} i_{d\_wm} \\ i_{q\_wm} \\ i_{d\_wr} \\ i_{q\_wr} \end{pmatrix} + \begin{pmatrix} \Psi_{fri} \\ 0 \\ \Psi_{fro} \\ 0 \end{pmatrix} \quad (17)$$

Then, voltage equation in  $d$ - $q$  reference frame can be expressed as:

$$\begin{cases} V_{d\_wm} = R_{s\_wm} i_{d\_wm} + p\Psi_{d\_wm} - (\omega_{ro} - \omega_{ri})\Psi_{q\_wm} \\ V_{q\_wm} = R_{s\_wm} i_{q\_wm} + p\Psi_{q\_wm} + (\omega_{ro} - \omega_{ri})\Psi_{d\_wm} \\ V_{d\_wr} = R_{s\_wr} i_{d\_wr} + p\Psi_{d\_wr} - \omega_{ro}\Psi_{q\_wr} \\ V_{q\_wr} = R_{s\_wr} i_{q\_wr} + p\Psi_{q\_wr} + \omega_{ro}\Psi_{d\_wr} \end{cases} \quad (18)$$

According to the aforementioned analysis of machine external characteristic, the electromagnetic torque on the inner and outer rotor can be expressed as (19). With this mathematical model, the control strategy based on vector control strategy can be developed and applied on the prototype.

$$\begin{cases} T_{e\_ri} = 1.5P_{ri} \cdot (\Psi_{d\_wm} i_{q\_wm} - \Psi_{q\_wm} i_{d\_wm}) \\ T_{e\_ro} = 1.5P_{ro} \cdot (\Psi_{q\_wm} i_{d\_wm} - \Psi_{d\_wm} i_{q\_wm}) + \\ 1.5 \cdot P_{ro} \cdot (\Psi_{d\_wr} i_{q\_wr} - \Psi_{q\_wr} i_{d\_wr}) \end{cases} \quad (19)$$

#### B. Control strategy under HEV operation condition

To obtain a precise control performance, the two rotors' position must be detected to implement field-oriented control. For the regular winding, it is designed as an auxiliary winding and its flux only couples with the outer rotor, therefore, the electrical angle for regular winding can be detected only through outer rotor resolver. However, the electrical angle for modulation winding is determined by the relative position of outer and inner rotor according to the equation (2), and can be obtained by (20).

$$\theta_{wm} = \theta_{ro} - \theta_{ri} \quad (20)$$

In the initial location of the rotors, a direct current is first injected into regular winding, outer rotor is forced to align with regular winding axis. Then another direct current is injected into modulation winding, which force inner rotor to align with virtual axis produced by modulator and modulation winding. It should be noted that although the two rotors may vibrate by cogging torque in the initial location process, this vibration cannot affect each other.

The whole basic control diagram based on field-oriented control strategy has been illustrated in Fig. 6. This control

diagram is only used in pure electrical drive mode. There are two control structures in the diagram, which control the outer and inner rotor speed, respectively. Each control structure is with a double-loop form, which is with a speed loop in the outside and a current loop in the inside. The positions of outer and inner rotor are detected simultaneously to close up modulation winding current loop.

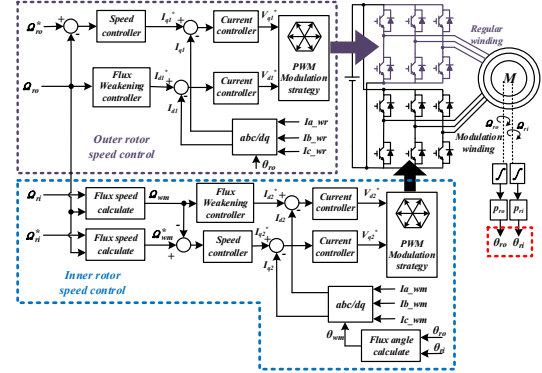


Fig. 6. The whole basic control diagram.

For normal hybrid electric drive operation, the control diagram can be changed into Fig. 7. Speed command of the outer and inner rotor are removed. The control instruction of the motor is given by an energy management unit. It decides the operation mode of the HEV and gives PWM control signal to the machine according to driver's instruction in the real time. The

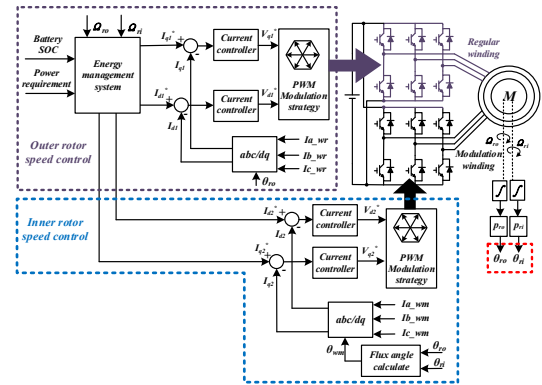


Fig. 7. Hybrid electric drive operation control diagram.

design of energy management is based on the whole vehicle test with optimization theory [31] [32], which is not elaborated here. Generally, according to the state of charge (SOC) of the battery and power requirement, the energy management system will give instructions of inner and outer rotor torque. Then, based on the characteristics of the machine (8) (9) (11) (19), the corresponding torque distributions of outer and inner rotor are calculated into current reference of two sets of windings, the diagram is shown in Fig. 8.

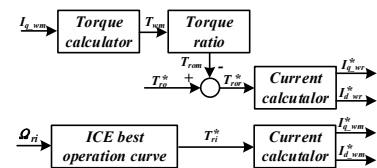


Fig. 8. Diagram of calculation of current reference.

#### IV. ANALYSIS OF ENERGY FLOW UNDER DIFFERENT WORKING CONDITIONS

Under the HEVs' normal operating conditions, the BLDD system is designed as an energy distribution unit. The proposed drive system diagram for this BLDD machine is shown in Fig. 9. It is constructed with a double three-phase half bridge structure converters. The two converters share a same DC bus bar, which is linked to battery through a DC/DC converter. Each AC/DC converter is connected to one set of winding to realize energy output or energy feedback. The function and mechanical connection of the two rotors is as follows: the outer rotor serves as the main drive rotor and is connected with reducer, and it is driving the wheels of HEV directly. While The inner rotor serves as a mechanical power input port and is connected to internal-combustion engine through a normal coupling to transmit mechanical energy to BLDD machine.

Normally, common operation mode under city road condition for hybrid vehicles is shown in Fig. 10. It can be figured that required output speed and torque are varied with HEV's different operation state. To keep ICE working along the maximum efficiency curve, the BLDD machine changes the torque and speed from the best efficiency point for ICE to the torque and speed required at reducer. In fact, for the real application, the ICE and battery have to be instructed to cooperate or work alone to supply output power of the whole car according to the road condition and vehicle's speed variations.

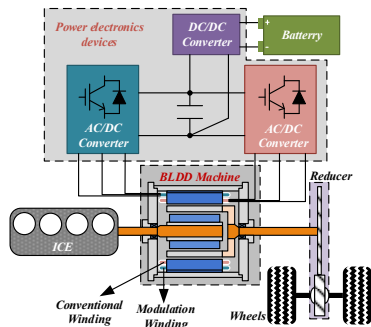


Fig. 9. Drive system for BLDD machine in hybrid electrical vehicles.

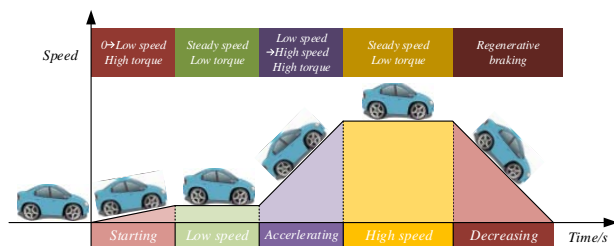


Fig. 10. Common operation mode for hybrid vehicles.

Different operation state of the HEV determines the two AC/DC converters' power flow. Here the positive direction of power is set as follows: for electrical pot, positive power represents power flowing from the battery to motor shaft; alternatively, the negative power represents power flowing from the motor shaft to battery.

When the car is running forward, the torque input from ICE  $T_{ri} > 0$ , according to (9),  $T_{wm} > 0$ . Since power is the product of

torque and speed, the power flow for modulation winding is determined by direction of the  $f_{wm}$ . Considering critical situation, when  $f_{ro} = f_{ri}$ , then  $f_{wm} = 0$ . At this moment, magnetic field produced by modulation winding is at standstill, even though outer rotor and inner rotor are rotating with the relationship  $\Omega_{ro}/\Omega_{ri} = p_{ri}/p_{ro}$ . The power flow for modulation winding is 0. Similarly, for regular winding, the machine outer rotor speed direction is fixed, i.e.  $f_{wr} = f_{ro} > 0$ , the power flow is determined by direction of the  $T_{ror}$ . According to this rule, the drive state of the system can be classified into following types:

##### 1) Pure electric drive

In this state, the HEV is driven by pure electrical energy from battery. The ICE is not working and detached from BLDD system. The modulation winding is in open circuit condition and the output shaft is mainly controlled by regular winding. So the whole machine is functioned as a conventional PM machine. The mechanical power and electrical power flow path are marked in Fig. 11.

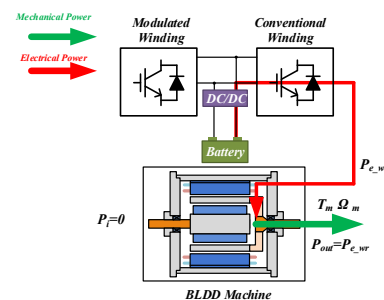


Fig. 11. State 1: Pure electrical drive.

##### 2) Pure engine drive

In this state, the HEV is driven by pure mechanical energy from the ICE. The electrical frequency of the outer and inner rotor meet the constraint  $f_{ro} = f_{ri}$ , while the torque on outer and inner rotor satisfy the equation  $T_{ro} = (p_{ro}/p_{ri})T_{ri}$ . The regular winding is in open circuit condition and the modulation winding is excited with proper  $i_q$  current to maintain the function of electromagnetic gear. Theoretically, the power of outer rotor and inner rotor are equal to each other, but the reality is that the main winding will still supply power for the copper loss and core loss. The mechanical power and electrical power flow path are marked in Fig. 12.

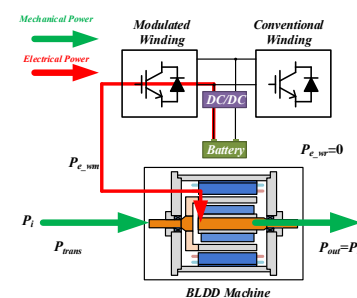


Fig. 12. State 2: Pure engine drive.

##### 3) Reduced speed and increased torque

In this state, the electrical frequency of the outer and inner rotor meet the constraint  $f_{ro} < f_{ri}$ , while torque on outer and inner rotor meet the constraint  $T_{ro} > (p_{ro}/p_{ri})T_{ri}$ . MGM is in the generator state while PMSM motor is in the motor state. The speed of the outer rotor is reduced and the torque is increased

compared to the inner rotor. The mechanical power and electrical power flow path are marked in Fig. 13. This state can be used in low speed and high torque working state of the HEV.

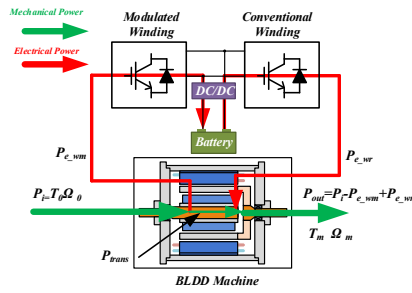


Fig. 13. State 2:  $f_{ro} < f_{ri}$ ,  $\frac{1+k}{k} T_{ri} < T_{ro}$ .

#### 4) Increased speed and increased torque

In this state, both the torque and speed are increased from ICE. The electrical frequency of outer and inner rotor meet the constraint  $f_{ro} > f_{ri}$ , and torque on outer and inner rotor meet the constraint  $T_{ro} > (p_{ro}/p_{ri})T_{ri}$ . MGM and PMSM motor are both in the motor state. The speed and torque of the outer rotor are both increased compared to the inner rotor. The mechanical power and electrical power flow path are marked in Fig. 14. The state can be chosen when high speed and high torque working state is required by the HEV.

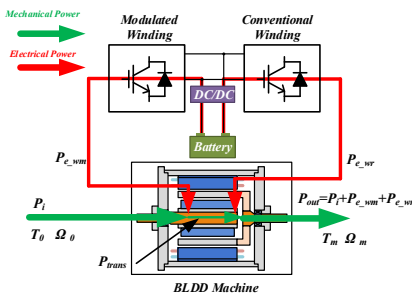


Fig. 14. State 3:  $f_{ro} > f_{ri}$ ,  $\frac{1+k}{k} T_{ri} < T_{ro}$ .

#### 5) Increased speed and reduced torque

In this state, electrical frequency of outer and inner rotor meet the constraint  $f_{ro} > f_{ri}$ , while  $T_{ro} < (p_{ro}/p_{ri})T_{ri}$ . MGM is in the motor state while PMSM motor is in the generator state. The BLDD system reduces the torque and increases speed from ICE. The mechanical power and electrical power flow path are marked in Fig. 15. Choosing this state means HEV is in the high speed and low torque working state.

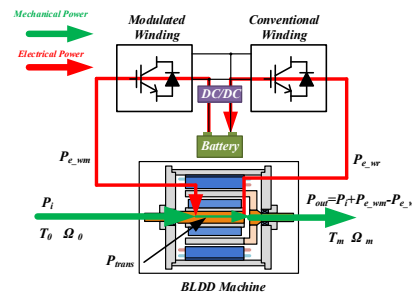


Fig. 15. State 4:  $f_{ro} > f_{ri}$ ,  $\frac{1+k}{k} T_{ri} > T_{ro}$ .

#### 6) Reduced speed and reduced torque

In this state, electrical frequency of outer and inner rotor meet the constraint  $f_{ro} < f_{ri}$ , and torque on outer and inner rotor meet the constraint  $T_{ro} < (p_{ro}/p_{ri})T_{ri}$ . MGM and PMSM motor are both in the generator state. The BLDD-PM machine system reduced both the torque and speed from ICE, the excess energy is flowing into battery through converters. The mechanical power and electrical power flow path are marked in Fig. 16. This state can be used when the HEV requires low speed and low torque of the output shaft.

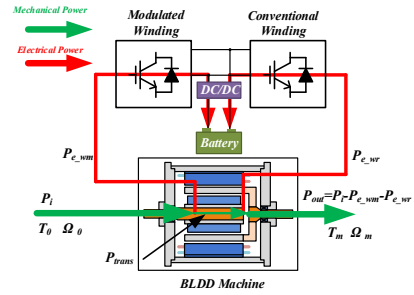


Fig. 16. State 5:  $f_{ro} < f_{ri}$ ,  $\frac{1+k}{k} T_{ri} > T_{ro}$ .

#### 7) Regenerative braking

In this state, ICE is shut down, remained kinetic energy on the input and output shaft will recharge the battery together through modulation winding and conventional winding. MGM and PMSM motor are in the generator state. The mechanical power and electrical power flow path are marked in Fig. 17.

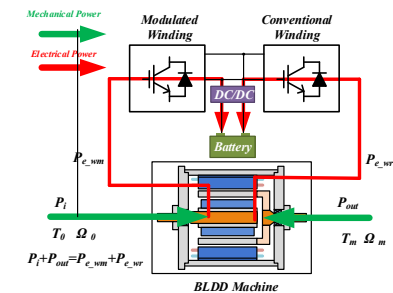


Fig. 17. State 6: Regenerative braking.

The total drive states of BLDD-PM machine system are shown in table II, where -1 stands for negative power state, 0 stands for not working and 1 stands for positive power state. It should be stressed that drive states of different operation condition are defined according to users' demand and can be used in combination.

TABLE II  
DRIVE MODE OF THE BLDD MACHINE

Modulation Winding	Conventional Winding	Drive Mode
-1	-1	$\Omega_o < \Omega_i$ , $T_o < T_i$
-1	1	$\Omega_o < \Omega_i$ , $T_o > T_i$
0	0	Stationary state
0	1	Pure electrical drive
1	-1	$\Omega_o > \Omega_i$ , $T_o < T_i$
1	0	Pure engine mode
1	1	$\Omega_o > \Omega_i$ , $T_o > T_i$

## V. HARDWARE AND EXPERIMENTS

To verify the analysis mentioned before and implement different function under different operation condition, the prototype and experiment platform has been designed and fabricated. The picture of stator core, rotor structure, and the whole machine are illustrated in Fig. 18. The whole picture of test bench is shown in Fig. 19. In this experiment, a servo motor is used to simulate the ICE and the servo motor is controlled with speed control mode to simulate one operation point of ICE at each time. The hardware of control system is shown in Fig. 20. The main control board is designed based on TI company TMS320F28377D chip and the main power circuit is designed based on Infineon FF300R17ME4 IGBT module along with its drive module. Under no load condition, steady state waveforms of back EMF tested with 0.5 rated speed of inner and outer rotor are shown in Fig. 21.

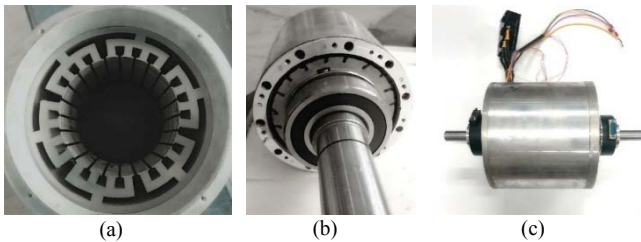


Fig. 18. Prototype of BLDD-PM used in the experiment: (a). Stator core. (b). Rotor structure. (c). Overall diagram.

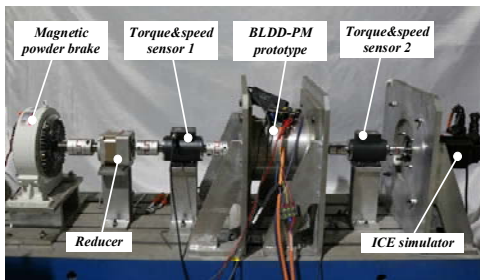


Fig. 19. BLDD-PM machine system test bench.

Fig. 22 gives the dynamic process of BLDD-PM system starting, when the machine is at pure electric drive operation. The outer rotor starts up and accelerate to 200 rpm with 5N.m load only through regular winding. The modulation winding does not work this time. It can be seen that the phase voltage and current of the regular winding are nearly in the same phase. It means regular winding is in the motor state.

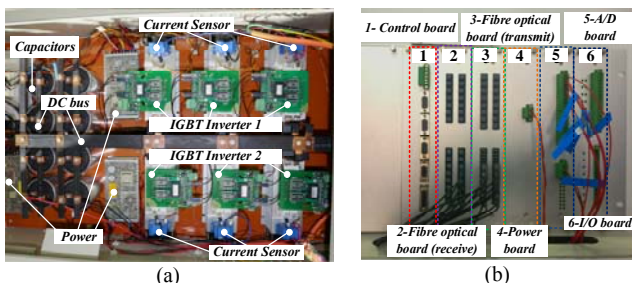


Fig. 20. Control system of BLDD-PM machine: (a). Main circuit based on Infineon IGBT module. (b). Control board based on TMS320F28377D.

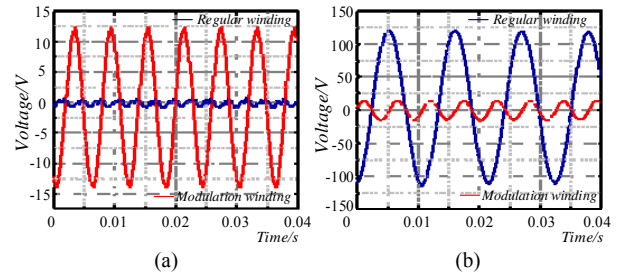


Fig. 21. No load back EMF tested with 0.5 rated speed of inner and outer rotor: (a). Outer rotor 500 rpm and inner rotor standstill. (b). Inner rotor 500 rpm and outer rotor standstill.

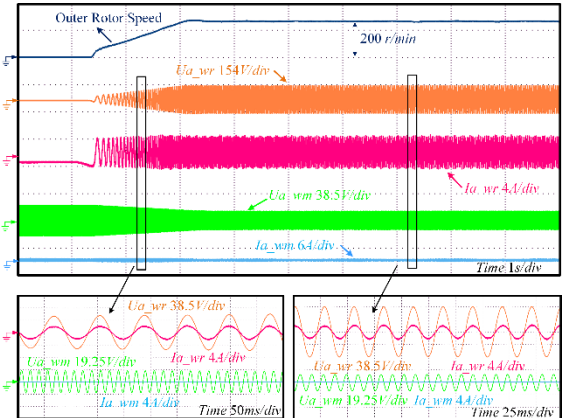


Fig. 22. Machine start from standstill to 200rpm with 5 N.m load in the experiment.

Fig. 23 shows the transient response to a sudden load torque reduction under low speed condition. In this state, the speed of outer rotor is kept a constant 200 rpm while the torque will endure a reduction. This state happens when the HEV has been started and gradually run at a low speed under smooth road condition. In the experiment, the ICE is linked into system with 500rpm and 5N.m, and the torque of outer rotor is 5.5 N.m at first and reduced to 2N.m later. From the picture, the phase of current and voltage of regular winding are nearly reversed after load reduction, which means regular winding return energy to DC bus. And modulation winding state keeps as the generator state during the whole process.

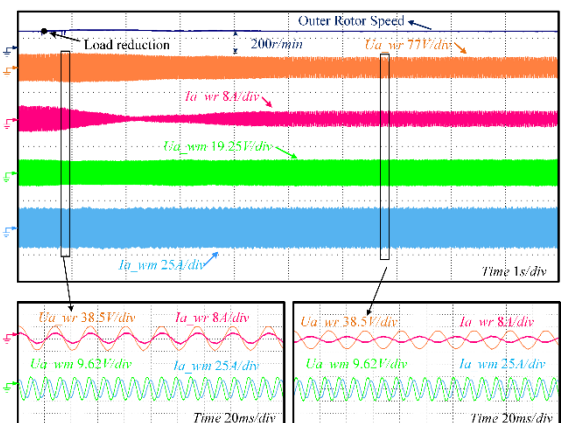


Fig. 23. Torque reduction of outer rotor from 5.5 N.m to 2 N.m when the outer rotor is kept 200 rpm in the experiment.

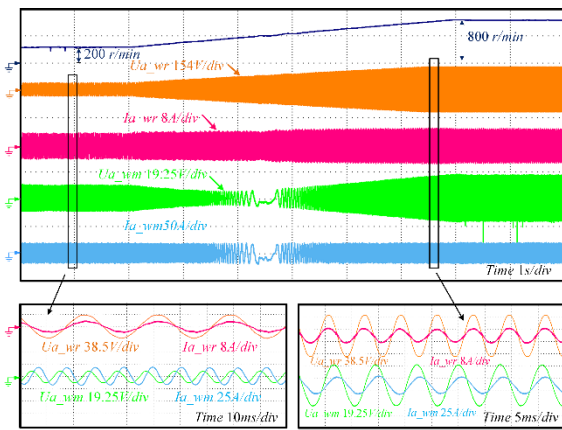


Fig. 24. Accelerate process from 200 rpm to 800 rpm with a 5 N.m load.

When the HEV is accelerating to a high speed, the torque and speed are boosted from ICE to reducing gear by BLDD machine system. The state of MGM and PMSM are both switched to motor mode. Fig 24 illustrates this process.

Fig. 25 shows the transient response to sudden load torque reduction under high speed condition. The outer rotor speed remains stable in the process. Different from Fig.23, the regular winding is switched to feedback energy state, while the modulation winding state is at motor state.

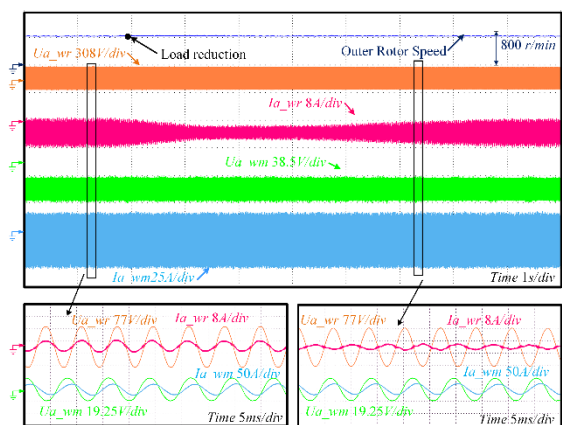


Fig. 25. Torque reduction of outer rotor from 5.5 N.m to 2 N.m when the outer rotor is kept 800 rpm in the experiment.

The deceleration process of the machine is shown in Fig. 26. In this state, the regular winding is required to work in generator state. The modulation winding is firstly maintaining the function of the electromagnetic gear, and then when the outer rotor speed has been reduced to low speed area, it begins to feedback the ICE mechanical energy to the DC bus. The mechanical energy stored on the rotating shaft is gradually transmitted to electrical energy in the DC or battery side.

Finally, the efficiency of the machine has been tested. In the experiment, the operation point of the ICE is fixed as 500 rpm and 4.5 N.m. Then, the speed and torque of the outer rotor have been changed to obtain the efficiency map, as it shown in Fig. 27. Because the machine is designed as a low-power prototype for principle verification, the rate of core loss, copper loss and switching loss are relatively higher, as a result, the efficiency of the machine is not so good.

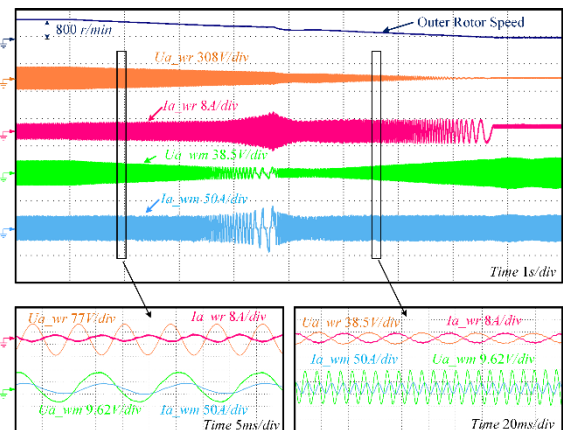


Fig. 26. The deceleration process in the experiment.

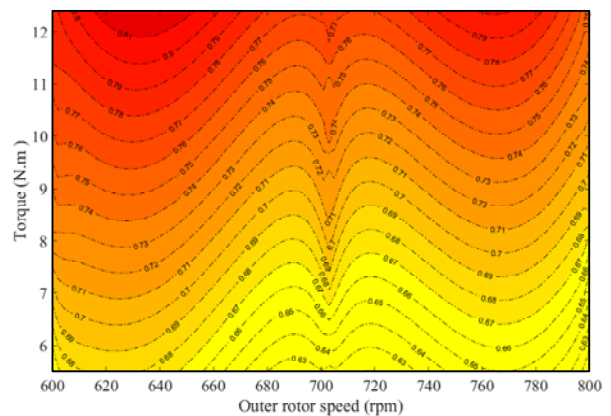


Fig. 27. Efficiency map of the machine.

## VI. CONCLUSIONS

BLDD-PM machine system can separate ICE and wheels through magnetic field, and can make ICE operate along the maximum efficiency curve under different road conditions. This paper gives an investigation of control strategy of this machine drive system and power flow under different operation state. Firstly, based on a new structure type, the operation principle and characteristic of this motor is illustrated. Then, the mathematical model of flux decoupled mathematical model of this motor together with its basic vector control strategy is developed. Next, according to common operation state of HEVs under city road condition, the power flow of the BLDD-PM machine system during different process has been analyzed. Finally, Experimental tests have been done on the BLDD-PM prototype. Here some conclusions can be derived:

- (1). BLDD-PM machine system can be totally regarded as a MGM and PMSM cascade through magnetic field.
- (2). By special design of the magnetic circuit, the two sets of windings in the stator side are decoupled, and can be controlled independently.
- (3). The electrical angle of rotating synchronous coordinate system for modulation winding is determined by the relative position of outer and inner rotor, and for regular winding is only determined by the position of outer rotor.
- (4). When ICE operates at fixed point, the power flow direction for modulation winding is determined by direction

of the  $f_{wm}$  and for regular winding is determined by direction of the  $T_{ror}$ .

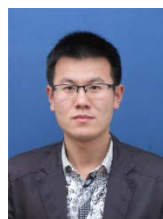
(5). Experimental test results under different operation condition show good control performance of the BLDD-PM prototype and verify the correctness of analysis.

## REFERENCES

- [1] M. Ehsani, Y. Gao, and J. M. Miller, "Hybrid electric vehicles: Architecture and motor drives," in *Proc. IEEE*, vol. 95, no. 4, pp. 719–728, Apr. 2007.
- [2] C. C. Chan, "The State of the Art of Electric, Hybrid, and Fuel Cell Vehicles" in *Proc. IEEE*, vol. 95, no. 4, pp. 704–718, Apr. 2007.
- [3] J. M. Miller, "Hybrid electric vehicle propulsion system architectures of the e-CVT type," in *IEEE Trans. Power Electron.*, vol. 21, no. 3, pp. 756–767, May 2006.
- [4] P. Han, M. Cheng and Zhe Chen, "Single-electrical-port control of cascaded doubly-fed induction machine for EV/HEV applications," *IEEE Trans. Power Electron.*, vol. 32, no. 9, pp. 7233–7243, Sep. 2017.
- [5] S. Eriksson and C. Sadarangani, "A four-quadrant HEV drive system," in *Proc. IEEE 56th Veh. Technol. Conf.*, Sep. 2002, vol. 3, pp. 1510–1514.
- [6] E. Nordlund and C. Sadarangani, "The four-quadrant energy transducer," in *Proc. Ind. Appl. Conf.*, Oct. 2002, pp. 390–397.
- [7] L. Xu, "A new breed of electric machines-basic analysis and applications of dual mechanical port electric machines," in *Proc. Int. Conf. Electr. Mach. Syst. (ICEMS)*, pp. 24–31, Sep. 2005.
- [8] P. Kececy and R. Lorenz, "Control methodology for single stator, dual rotor induction motor drives for electric vehicles," in *Proc. 26th Annu. IEEE Power Electron. Spec. Conf.*, vol. 2, Jun. 1995, pp. 572–578.
- [9] C. D. Tong, P. Zheng, Q. Wu, J. G. Bai, and Q. B. Zhao, "A brushless claw-pole double-rotor machine for power-split hybrid electric vehicles," in *IEEE Trans. Ind. Electron.*, vol. 61, no. 8, pp. 4295–4305, Aug. 2014.
- [10] A. Sant, V. Khadkikar, W. Xiao, and H. Zeineldin, "Four-axis vector controlled dual-rotor PMSM for plug-in electric vehicles," in *IEEE Trans. Ind. Electron.*, vol. 62, no. 5, pp. 3202–3212, May 2015.
- [11] K. T. Chau, C. C. Chan, and C. Liu, "Overview of permanent-magnet brushless drives for electric and hybrid electric vehicles," in *IEEE Trans. Ind. Electron.*, vol. 55, no. 6, pp. 2246–2257, Jun. 2008.
- [12] M. Venturini and F. Leonardi, "High torque, low speed joint actuator based on PM brushless motor and magnetic gearing," in *Rec. IEEE IAS Annu. Meeting*, pp. 37–42, Oct. 1993.
- [13] A. Toba and T. Lipo, "Generic torque-maximizing design methodology of surface permanent-magnet vernier machine," in *IEEE Trans. Ind. Appl.*, vol. 36, no. 6, pp. 2032–2035, Jun. 2005.
- [14] B. Kim, and T. Lipo, "Operation and design principles of a PM vernier motor," in *IEEE Trans. Ind. Appl.*, vol. 50, no. 6, pp. 3656–3663, Nov./Dec. 2014.
- [15] A. Ishizaki, et al., "Theory and optimum design of PM vernier motor," in *Proc. IEE Int. Conf. Electrical Machines and Drives '95*, 1995, pp. 208–212.
- [16] D. Li, R. Qu, J. Li, L. Wu and W. Xu, "Analysis of torque capability and quality in vernier permanent magnet machines," *IEEE Trans. Ind. Appl.*, vol. 52, no. 1, pp. 125–135, Jan./Feb. 2016.
- [17] D. Li, R. Qu, and T. Lipo, "High-power-factor vernier permanent-magnet machines," *IEEE Trans. Ind. Appl.*, vol. 50, no. 6, pp. 3664–3674, Nov./Dec. 2014.
- [18] L. Sun, M. Cheng and M. Tong, "Key Issues in Design and Manufacture of Magnetic-Geared Dual-Rotor Motor for Hybrid Vehicles," in *IEEE Transactions on Energy Conversion*, vol. 32, no. 4, pp. 1492–1501, Dec. 2017.
- [19] A. Ghayebloo and A. Radan, "Superiority of Dual-Mechanical-Port-Machine-Based Structure for Series-Parallel Hybrid Electric Vehicle Applications," in *IEEE Transactions on Vehicular Technology*, vol. 65, no. 2, pp. 589–602, Feb. 2016.
- [20] Y. Liu, D. Cheng, Y. Sui, J. Bai, C. Tong and W. Tong, "Magnetic System Study of a Compound-Structure Permanent-Magnet Synchronous Machine for HEVs," in *IEEE Transactions on Industry Applications*, vol. 48, no. 6, pp. 1797–1807, Nov.-Dec. 2012.
- [21] L. Sun, M. Cheng, H. Wen and L. Song, "Motion Control and Performance Evaluation of a Magnetic-Geared Dual-Rotor Motor in Hybrid Powertrain," in *IEEE Transactions on Industrial Electronics*, vol. 64, no. 3, pp. 1863–1872, March 2017.
- [22] L. Tang and G. J. Su, "High-Performance Control of Two Three-Phase Permanent-Magnet Synchronous Machines in an Integrated Drive for Automotive Applications," in *IEEE Transactions on Power Electronics*, vol. 23, no. 6, pp. 3047–3055, Nov. 2008.
- [23] Y. Tang, Dual motor drive and control system for an electric vehicle, US Patent 2010022953 A1, Tesla Motors, Inc., Sep. 2010.
- [24] L. Xu, Y. Zhang and X. Wen, "Multi-operational modes and control strategies of dual-mechanical-port machine for hybrid electrical vehicles," in *IEEE Trans. Ind. Appl.*, vol. 45, no. 2, pp. 747–755, Mar./Apr. 2009.
- [25] X. Luo and S. Niu, "A Novel Contra-Rotating Power Split Transmission System for Wind Power Generation and Its Dual MPPT Control Strategy," in *IEEE Transactions on Power Electronics*, vol. 32, no. 9, pp. 6924–6935, Sept. 2017.
- [26] G. Zhang et al., "A Robust Control Scheme Based on ISMC for the Brushless Doubly Fed Induction Machine," in *IEEE Transactions on Power Electronics*, vol. 33, no. 4, pp. 3129–3140, April 2018.
- [27] D. Li, R. Qu, X. Ren and Y. Gao, "Brushless dual-electrical-port, dual mechanical port machines based on the flux modulation principle," in *Proc. IEEE Energy Convers. Congr. Expo*, 2016.
- [28] Y. Wang, S. Niu and W. Fu, "Electrical-Continuously Variable Transmission System Based on Doubly Fed Flux-Bidirectional Modulation," in *IEEE Transactions on Industrial Electronics*, vol. 64, no. 4, pp. 2722–2731, April 2017.
- [29] S. Niu, S. L. Ho, and W. N. Fu, "Design of a novel electrical continuously variable transmission system based on harmonic spectra analysis of magnetic field," in *IEEE Trans. Magn.*, vol. 49, no. 5, pp. 2161–2164, May 2013.
- [30] X. Ren, D. Li, R. Qu and T. Zou, "A Brushless Dual-Mechanical-Port Dual-Electrical-Port Machine With Spoke Array Magnets in Flux Modulator," in *IEEE Transactions on Magnetics*, vol. 53, no. 11, pp. 1–6, Nov. 2017.
- [31] J. Moreno, M. E. Ortuzar and J. W. Dixon, "Energy-management system for a hybrid electric vehicle, using ultracapacitors and neural networks," in *IEEE Transactions on Industrial Electronics*, vol. 53, no. 2, pp. 614–623, April 2006.
- [32] P. Pisu and G. Rizzoni, "A Comparative Study Of Supervisory Control Strategies for Hybrid Electric Vehicles," in *IEEE Transactions on Control Systems Technology*, vol. 15, no. 3, pp. 506–518, May 2007



**Xun Han** (S'17) was born in Hubei, China in 1992. He received the B.E.E. degree in electrical and electronic engineering, from Harbin Institute of Technology at Weihai, Weihai, China, in 2015. He is currently working toward the Ph.D. degree in the School of Electrical and Electronic Engineering, Huazhong University of Science and Technology, Wuhan, China. His research interests include the control of novel permanent magnet machines and power electronics.



**Wubin Kong** (M'15) was born in Zhejiang, China, in 1986. He received the B.S. and Ph.D. degree in electrical engineering from Zhejiang University, Hangzhou, China in 2009 and 2014, respectively. His research interests are high-power multiphase motor drives and fault tolerant control motor drive applied in EV. From 2015, he has been a lecture with Huazhong University of Science & Technology, Wuhan, China.



**Ronghai Qu** (S'01–M'02–SM'05–F'18) was born in China. He received the B.E.E. and M.S.E.E. degrees from Tsinghua University, Beijing, China, and the Ph.D. degree from the University of Wisconsin–Madison, Madison, WI, USA, in 1993, 1996, and 2002, respectively, all in electrical engineering.

In 1998, he joined the Wisconsin Electric Machines and Power Electronics Consortiums, University of Wisconsin–Madison, WI, USA, as a Research Assistant. He became a Senior Electrical Engineer at Northland, a Scott Fetzer Company, Watertown, NY, USA, in 2002. Since 2003, he has been with the General Electric (GE) Global Research Center, Niskayuna, NY, USA, as a Senior Electrical Engineer in the Electrical Machines and Drives Laboratory. He has authored more than 230 published technical papers and is the holder

of more than 50 patents/patent applications. Since 2010, he has been a Professor with Huazhong University of Science and Technology, Wuhan, China. Dr. Qu is a full member of Sigma Xi. He has received several awards from the GE Global Research Center since 2003, including the Technical Achievement and Management Awards. He also received the 2003 and 2005 Best Paper Awards, third prize, from the Electric Machines Committee of the IEEE Industry Applications Society (IAS) at the 2002 and 2004 IAS Annual Meeting, respectively.



**Dawei Li** (S'12-M'15) was born in China. He received the B.E.E. degrees in electrical engineering from Harbin Institute of Technology, Harbin, China, in 2010 and the Ph.D. degree in electrical engineering from Huazhong University of Science & Technology, in 2015. In Jul. 2015, he joined Huazhong University of Science & Technology, Wuhan, China. Dr. Li has authored over 60 published technical papers and is the holder of over 10 patents/patent applications. He was recipient of the Best

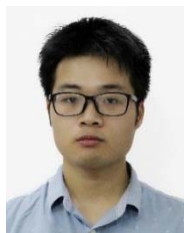
Poster Presentation Award from the XXII th International Conference on Electrical Machines (ICEM 2016), and Hubei Province Excellent Doctoral Dissertation (2016), China. His research areas include the design and analysis of flux-modulation permanent-magnet brushless machines.



**Tianjie Zou** (S' 15) was born in Hubei, China in 1991. He received the B.E.E. degree in electrical and electronic engineering, from Huazhong University of Science and Technology, Wuhan, China, in 2013, where he is currently working towards his Ph.D. degree in electrical engineering. His main research interests include design, analysis and intelligent control of permanent-magnet machines.



**Xiang Ren** was born in Hunan, China. He received the B.S. degree in mechanical engineering from Huazhong University of Science and Technology, Wuhan, China, in 2014. He is currently working toward the Ph.D. degree in Huazhong University of Science and Technology in electrical engineering. His research interests include design and analysis of flux modulation machines.



**Tonghao Pei** (S' 16) was born in Wenzhou, China in 1994. He received the B.E.E. degree from Zhejiang Sci-Tech University, Hangzhou, China, in 2016. And he is currently working towards his master degree in electrical engineering at Huazhong University of Science and Technology. His main research interests include design, analysis and optimizing of permanent-magnet machines.



**Kai Yang** received the B.Eng., M.Sc., and Ph.D. degrees in electrical and electronic engineering from Huazhong University of Science and Technology, Wuhan, China, in 1998, 2000, and 2003, respectively. He is a Professor with the College of Electrical and Electronic Engineering, Huazhong University of Science and Technology, and the Director of the Department of Electrical Machinery and Control. His research interests include new type motors and their servo control systems.



**Chun Gan** (S'14-M'16) received B.S. and M.S. degrees in power electronics and motor drives from China University of Mining and Technology, Jiangsu, China, in 2009 and 2012, respectively, and Ph.D. degree in power electronics and motor drives from Zhejiang University, Hangzhou, China, in 2016. He is currently a research associate in Department of Electrical Engineering and Computer Science, The University of Tennessee, Knoxville, Tennessee, USA. He is also a member of the U.S. Energy/National Science Foundation cofounded Engineering Research Center. He has published more than 40 technical papers in leading journals and conference proceedings, and authored one book chapter. He has ten issued/published invention patents. His research interests include high-efficiency power converters, electric vehicles, electrical motor drives, electrical motor design, continuous variable series reactor, high voltage direct current transmission, and micro-grid.